J|A|C|S
ARTICLES

Published on Web 01/30/2009

Electrolyte-Dependent Electrosynthesis and Activity of Cobalt-Based Water Oxidation Catalysts

Yogesh Surendranath, Mircea Dincă, and Daniel G. Nocera*

Department of Chemistry, 6-335, Massachusetts Institute of Technology, Cambridge, Massachusetts 02139-4307

Received October 2, 2008; E-mail: nocera@mit.edu

Abstract: Electrolysis of Co^{2+} in phosphate, methylphosphonate, and borate electrolytes effects the electrodeposition of an amorphous highly active water oxidation catalyst as a thin film on an inert anode. Electrodeposition of a catalytically competent species immediately follows oxidation of Co^{2+} to Co^{3+} in solution. Methylphosphonate and borate electrolytes support catalyst activity comparable to that observed for phosphate. Catalytic activity for O_2 generation in aqueous solutions containing 0.5 M NaCl is retained for catalysts grown from phosphate electrolyte.

Introduction

The solar-driven electrochemical splitting of water to produce hydrogen and oxygen provides an effective means of energy storage.[1,2] This water-to-solar fuels conversion requires proton-coupled multielectron oxidation of water to O_2 with the release of four protons and their subsequent reduction to H_2. Of these two processes, the oxidation reaction is particularly demanding[3,4] because it requires the removal of four protons and four electrons and the formation of an oxygen−oxygen double bond. Commercial electrolyzers perform the water-splitting reaction at high efficiency and current density, but this technology is not well matched to conditions of many envisioned nonconcentrated (e.g., distributed) solar applications.[5] In these electrolyzers, the water-splitting reaction is performed under harsh physical and chemical conditions and the systems are expensive. We have turned our attention to developing water-splitting catalysts for inexpensive and highly manufacturable nonconcentrated solar applications. A recent report from our laboratory shows that the electrolysis of Co^{2+} salts in pH 7 phosphate electrolyte (Pi) effects the electrodeposition of a highly active water oxidation catalyst as an amorphous thin film on an inert indium−tin−oxide (ITO) or fluorine−tin−oxide (FTO) electrode.[6] In contrast to spinel and perovskite metal oxides that oxidize water under highly alkaline conditions,[7] the electrodeposited cobalt−phosphate compound is among the few catalysts for which activity at neutral pH has been demonstrated,[8,9] and among these, it is unique because it does not involve a precious metal constituent.

We now elaborate the design of the system in two ways: (1) catalyst formation and function is not restricted to Pi; a fully functional catalyst is formed from a methylphosphonate (MePi) or borate (Bi) electrolyte; and (2) oxygen production from the electrodeposited catalyst is not impeded by the presence of chloride, allowing efficient oxygen evolution from salt water. The activity of the catalyst is evaluated in comparison to materials deposited from electrolytes that are poor proton acceptors at neutral pH. In the absence of proton-accepting electrolytes: (1) catalyst formation is significantly impeded at a given potential and is not observed under conditions similar to those employed for Co−Pi, Co−MePi, or Co−Bi catalysts; (2) catalyst activity is severely diminished and deteriorates over time; and (3) chloride oxidation out-competes water oxidation from salt solutions. These results together establish the imperative for proton-accepting electrolytes, which enable catalyst formation, sustained activity, and functional stability.

Results

Cyclic Voltammetry. Cyclic voltammetry (CV) scans of a glassy carbon working electrode in an aqueous 0.5 mM Co^{2+} solution in 0.1 M potassium phosphate electrolyte at pH 7.0 (Pi), 0.1 M sodium methylphosphonate electrolyte at pH 8.0 (MePi), and 0.1 M potassium borate electrolyte at pH 9.2 (Bi) are shown in Figure 1 along with the respective background traces taken in pure electrolyte with no Co^{2+}. As reported previously,[6] in Pi electrolyte a sharp anodic wave is observed at $E_{p,a} = 1.13$ V vs NHE, followed by a strong catalytic wave at 1.23 V. The corresponding sharp anodic wave in MePi is observed at $E_{p,a} = 1.04$ V, followed by the onset of a catalytic wave at 1.14 V. In Bi electrolyte, the anodic wave is observed at $E_{p,a} = 0.77$ V and is well separated from the catalytic wave at 1.10 V. A catalytic current of 100 μA is observed at 1.34, 1.27, and 1.20 V for Pi, MePi, and Bi electrolytes, respectively. The 70 mV shift between MePi and Bi reflects the 72 mV shift in the thermodynamic potential for water oxidation between pH 8.0 and 9.2. A broad cathodic wave at $E_{p,c} = 0.93$, 0.81, and

(1) Lewis, N. S.; Nocera, D. G. *Proc. Natl. Acad. Sci. U.S.A.* **2006**, *103*, 15729.
(2) Dempsey, J. L.; Esswein, A. J.; Manke, D. R.; Rosenthal, J.; Soper, J. D.; Nocera, D. G. *Inorg. Chem.* **2005**, *44*, 6879.
(3) Eisenberg, R.; Gray, H. B. *Inorg. Chem.* **2008**, *47*, 1697.
(4) Betley, T. A.; Wu, Q.; Van Voorhis, T.; Nocera, D. G. *Inorg. Chem.* **2008**, *47*, 1849.
(5) Turner, J. A. *Science* **1999**, *285*, 5428.
(6) Kanan, M. W.; Nocera, D. G. *Science* **2008**, *321*, 1072.
(7) Tarasevich, M. R.; Efremov B. N. In *Electrodes of Conductive Metal Oxides*; Trasatti, S., Ed.; Elsevier: Amsterdam, 1980; Chapter *5*.
(8) Yagi, M.; Tomita, E.; Sakita, S.; Kuwabara, T.; Nagai, K. *J. Phys. Chem. B.* **2005**, *109*, 21489.
(9) Hara, M.; Waraksa, C. C.; Lean, J. T.; Lewis, B. A.; Mallouk, T. E. *J. Phys. Chem. A* **2000**, *104*, 5275.

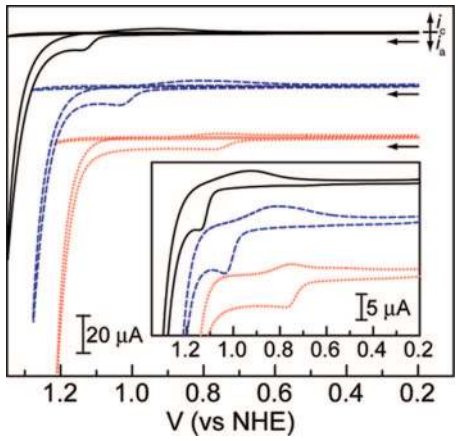

Figure 1. Cyclic voltammogram using a glassy carbon working electrode, 50 mV/s scan rate, of aqueous 0.5 mM Co^{2+} in 0.1 M Pi electrolyte, pH 7.0 (—, black), 0.1 M MePi electrolyte, pH 8.0 (- - -, blue), and 0.1 M Bi electrolyte, pH 9.2 (•••, red). Background traces in each electrolyte medium in the absence of Co^{2+} are overlaid. Inset shows CVs in the presence of Co^{2+} on an expanded current scale.

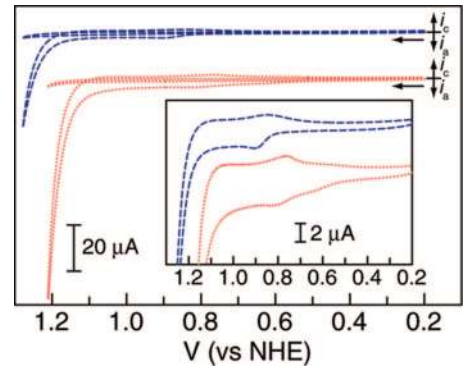

Figure 2. Cyclic voltammogram using a glassy carbon working electrode, 50 mV/s scan rate, in 0.1 M MePi electrolyte, pH 8.0 (- - -, blue), and 0.1 M Bi electrolyte, pH 9.2 (•••, red), with no Co^{2+} present after 1 scan in the presence of 0.5 mM Co^{2+}. Background scan of a freshly polished electrode is overlaid. Inset shows CVs on an expanded current scale.

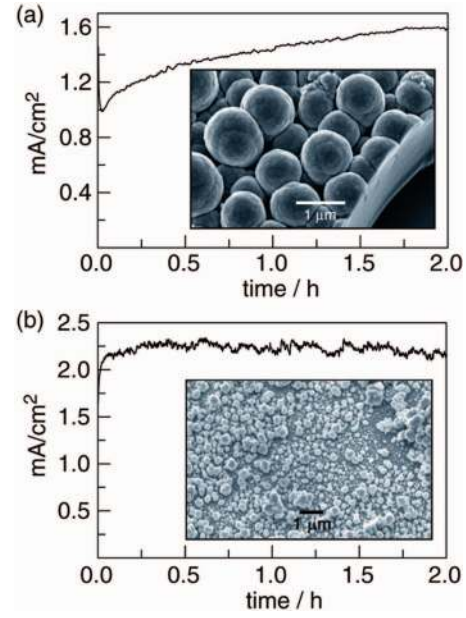

Figure 3. Current density trace for bulk electrolysis at 1.30 V in 0.1 M MePi electrolyte, pH 8.0, 1 mM Co^{2+} on an ITO anode (a) and for bulk electrolysis at 1.30 V in 0.1 M Bi electrolyte, pH 9.2, 0.5 mM Co^{2+} (b). Insets: SEM images (30° tilt) of catalyst films electrodeposited from (a) MePi electrolyte and (b) Bi electrolyte.

0.55 is observed in Pi, MePi, and Bi, respectively; for the latter electrolyte, the cathodic wave is also followed by a broad cathodic shoulder. On subsequent scans, the sharp anodic prefeature of all electrolyte solutions is replaced by a broad anodic wave that grows upon repetitive scanning suggesting adsorption of an electroactive species (Figure S1, inset).

The phenomenon of electrodeposition was probed further in MePi and Bi electrolytes where the anodic prefeature is well separated from the catalytic wave. A single CV scan of a polished glassy carbon electrode was performed in solutions of 0.5 mM Co^{2+} in MePi and Bi electrolytes, and the scan was reversed beyond the anodic prefeature wave but prior to the catalytic wave. The electrode was removed from solution, rinsed with water, and placed in fresh electrolyte solution containing no Co^{2+}. The subsequent CV scans of the electrode in MePi and Bi are shown in Figure 2. For both electrolytes, a strong catalytic wave is observed.

Film Preparation and Characterization. To investigate the nature of the catalytic wave, controlled potential electrolysis was performed at 1.3 V in a conventional two-compartment cell. In each case, the working compartment was charged with either a 1 mM Co^{2+} solution in MePi electrolyte or a 0.5 mM Co^{2+} solution in Bi electrolyte, whereas the auxiliary compartment was charged with pure electrolyte. ITO-coated glass slides were used as working electrodes in each case. In MePi, the current density reaches an asymptotic limit of 1.5 mA/cm^2 over the course of 2 h (Figure 3a). In Bi, the current density reaches an asymptotic limit of 2.3 mA/cm^2 over the course of 10 min (Figure 3b). In both cases, the sustained current is accompanied by the formation of a dark green film on the ITO electrode and O_2 effervescence (vide infra).

The morphologies of films from Pi, MePi, and Bi electrolytes (Co−Pi, Co−MePi, and Co−Bi, respectively) have been analyzed by scanning electron microscopy. Depositions from MePi electrolyte were conducted from quiescent solutions. Progressively thicker films are observed at longer deposition times. Early in the course of electrolysis, a film of uniform ~1 μm thickness is observed upon passage of 6 C/cm^2 (Figure S2). Prolonged electrolysis (passage of 40 C/cm^2) produces a film ~3 μm thick with the concomitant formation of spherical nodules of 1−5 μm in diameter on the surface of the film (Figure 3a, inset). These morphological features are similar to those of films deposited from Pi electrolyte.[6] Depositions from Bi electrolyte under quiescent conditions lead to a rapid decrease of current arising from local pH gradients and associated resistive losses due to the formation of neutral H_3BO_3 species (Figure S8). As such, bulk electrolyses in Bi electrolyte were conducted with stirring, whereupon stable currents were observed for hours, as shown in Figure 3b. Unlike Co−Pi or Co−MePi, Co−Bi displays a somewhat different surface morphology. Spherical nodules appear early in the course of deposition (upon passage of 2 C/cm^2, Figure S3) and merge into larger aggregates upon prolonged electrolysis, as shown in the inset of Figure 3b. SEM images of Co−Bi films grown from quiescent solutions also reveal similar morphological features.

Powder X-ray diffraction patterns of Co−MePi and Co−Bi exhibit only broad amorphous features and no detectable crystallites besides those corresponding to the ITO substrate (Figure S4). In line with this observation, transmission electron

Table 1. Elemental Composition of Catalyst Films

deposition conditions	Co	P	Na	C	B	K
MePi, pH 8.0, 1 mM Co^{2+}	4.5	1	1.2	0.6		
MePi, pH 8.0, 10 mM Co^{2+}	4.5	1	0.9	0.8		
MePi, pH 7.0, 10 mM Co^{2+}	5.6	1	0.6	0.7		
Bi, pH 9.2, 0.5 mM Co^{2+}	9.5				1	1.0
Pi, pH 7.0, 0.5 mM Co^{2+}	2.7	1				1.0

microscopy of Co–Pi films does not reveal crystalline domains nor are electron diffraction spots observed on a length scale of 5 nm (Figure S5). The chemical compositions of the films were determined by elemental analysis and energy dispersive X-ray analysis (EDX). Catalyst films were electrodeposited on large surface area electrodes (as large as 20 cm × 20 cm) and the catalyst was removed from the surface to furnish up to 100 mg of black powder whose composition was determined by microanalysis. The mole ratios of the species present in the film for all deposition conditions attempted are shown in Table 1. Regardless of Co^{2+} concentration, Co−MePi films exhibit a Co/P ratio of 4.5:1, while lowering the pH to 7.0 caused a slight increase in the Co/P ratio. The elemental analysis data are corroborated by EDX analysis, which reveals Co/P ratios of 4:1 to 6:1 (Figure S6) for films that ranged in thickness from ∼100 nm to >3 μm, as well as for those prepared using Co^{2+} concentrations ranging from 0.1 to 10 mM. For Co−Bi films, a Co/B ratio of ∼10:1 is observed by elemental analysis.

Water Oxidation Catalysis and Activity. Mass spectrometry establishes that gas effervescence from the electrode is a result of O_2 production from water. The provenance of O_2 was determined by using ^{18}O-labeled water. MePi enriched with 18.9% $^{18}OH_2$ was chosen as a representative electrolyte. Evolved gases were detected in real time by mass spectrometry (Figure 4). Signals for all three isotopes of O_2 rise from their baseline levels minutes after the onset of electrolysis and then slowly decay after electrolysis is terminated and O_2 is purged from the head space. Notwithstanding, the same ratio of isotopes is preserved throughout. The observed isotopic ratio of 66.0:30.4:3.6 = $^{16,16}O_2/^{18,16}O_2/^{18,18}O_2$ is in good agreement with the predicted statistical ratio of 65.8:30.6:3.6 = $^{16,16}O_2/^{18,16}O_2/^{18,18}O_2$. A small amount of CO_2 (∼0.5%) is also observed, suggesting the oxidation of MePi to Pi within the catalyst film. In line with this contention, a ^{31}P NMR spectrum of dissolved films of the catalyst shows a phosphate/methylphosphonate ratio of ∼3:1 (Figure S9). The oxidation of MePi within the film is also reflected by a P/C ratio of ∼2:1 as determined by microanalysis. The lower carbon content observed by ^{31}P NMR relative to elemental analysis is attributed to the longer electrolysis time that was used for the NMR study. The issue of CO_2 evolution is obviated upon the replacement of MePi electrolyte with Bi or Pi electrolytes.

Whereas MePi is partially degraded within the film, NMR of the MePi electrolyte solution does not reveal decomposition of the electrolyte under prolonged electrolysis. Bulk electrolysis was conducted using an ITO anode and a 1 mM Co^{2+} solution. A charge of 87 C (1.8 equiv vs MePi; 180 equiv vs Co^{2+}) was passed and the solution from the working compartment of the electrochemical cell showed a single ^{31}P signal at 24.9 ppm (pH 6.3) and an ^1H signal at 1.22 ppm (J = 16.5 Hz). These values are similar to that of fresh electrolyte, which exhibits a ^{31}P signal at 21.8 ppm (pH 8.0) and a ^1H signal at 1.05 ppm (J = 15.5 Hz). No other major signals are observed in the NMR spectrum

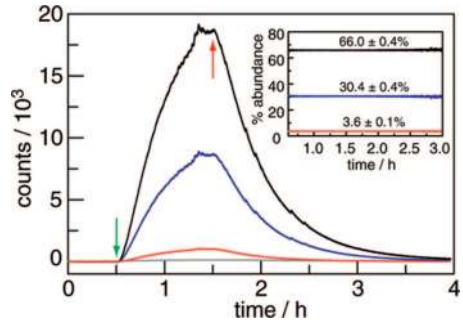

Figure 4. Mass spectrometric detection of isotopically labeled $^{16,16}O_2$ (top trace, black), $^{16,18}O_2$ (top middle trace, blue), $^{18,18}O_2$ (bottom middle trace, red), and CO_2 (bottom trace, gray) during electrolysis of a catalyst film on ITO in 0.1 M MePi electrolyte, pH 8.0, containing 18.9% $^{18}OH_2$. Green and red arrows indicate start and end of electrolysis, respectively. Inset: Percent abundance of each isotope over the course of the experiment. Average observed abundance ± 2σ indicated above each line. Statistical abundances: 65.8%, 30.6%, and 3.6%.

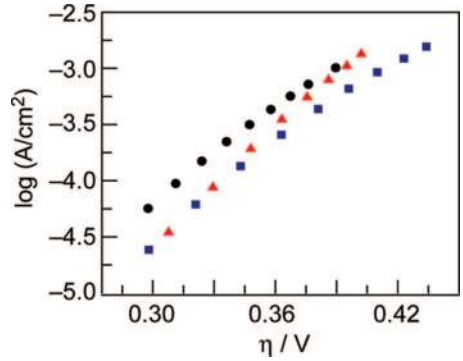

Figure 5. Tafel plot, $\eta = (V_{appl} - IR - E^\circ)$, of a catalyst film deposited from and operated in 0.1 M Pi electrolyte, pH 7.0 (●), 0.1 M MePi electrolyte, pH 8.0 (■), and 0.1 M Bi electrolyte, pH 9.2 (▲).

of solutions from either the working or auxiliary compartment (see Figure S10).

The Faradaic efficiency of catalysis was determined by fluorescence-based O_2 sensing of the evolved gases. In a bulk electrolysis using MePi, the amount of O_2 produced (145 μmol) accounted for 98(±5)% of the current passed (57 C; 148 μmol). For a Bi electrolyte, the amount of O_2 produced (135 μmol) accounted for 104(±5)% of the current passed (50 C; 130 μmol).

The log of current density versus overpotential relationship (Tafel plot) was used to evaluate the activity of catalysts grown from MePi and Bi electrolytes. Tafel plots data for Co−Pi, Co−MePi, and Co−Bi catalysts in their native electrolytes (Figure 5) are similar in slope, indicating that each of the electrolyte environments is equally competent at shuttling protons during catalytic turnover to sustain high activity.

Catalyst Electrodeposition and Activity in Nonbuffering Electrolytes. To assess the role of the electrolyte in catalyst formation and activity, experiments were performed in solutions containing Co^{2+} and electrolytes that are poor proton acceptors (e.g., SO_4^{2-}, NO_3^-, ClO_4^-). CVs of a glassy carbon working electrode in 0.1 M K_2SO_4 at pH 7.0, containing varying concentrations of Co^{2+} are shown in Figure 6. The first and fifth CV scans, taken without pause, are displayed along with the corresponding traces of a 0.5 mM Co^{2+} solution in Pi electrolyte. The CV traces of 0.5 mM Co^{2+} in the 0.1 M K_2SO_4 solution are indistinguishable from the background scan in the absence of Co^{2+} whereas a slight current enhancement over background is observed at 1.56 V from 5 mM Co^{2+} solutions.

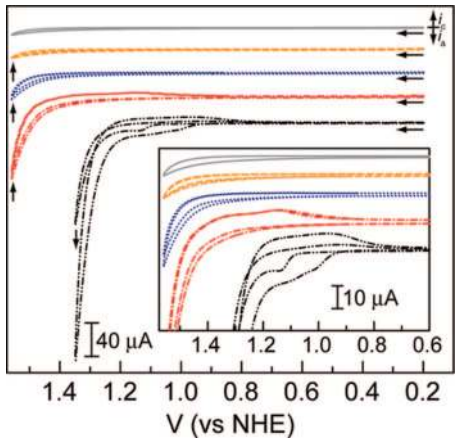

Figure 6. Cyclic voltammogram using a glassy carbon working electrode, 50 mV/s scan rate, of 0.1 M K_2SO_4 electrolyte, pH 7.0, containing from top to bottom 0 mM Co^{2+} (—), 0.5 mM Co^{2+} (- - -), 5 mM Co^{2+} (•••), and 50 mM Co^{2+} (−•−). CV traces of glassy carbon working electrode, 50 mV/s scan rate, of 0.5 mM Co^{2+} in Pi electrolyte, pH 7.0 (−••−) are shown for comparison. Vertical arrows indicated progression between the first and fifth scans taken without pause. Inset shows all CVs on an expanded current and potential scale.

At 50 mM Co^{2+}, a pronounced anodic wave, with an onset of 1.40 V, is observed. At this concentration, the return scan exhibits a small cathodic wave at $E_{p,c} = 1.15$ V. CVs recorded on Co^{2+} in K_2SO_4 solution exhibit slightly diminished currents on subsequent scans, contrasting those recorded in Pi electrolyte solution from which pronounced current enhancements are observed upon subsequent scanning. The same behavior is observed when 0.1 M $NaClO_4$, pH 7.0, is substituted for K_2SO_4 as the electrolyte (Figure S11). Hence, in electrolytes that are poor proton acceptors, catalyst formation does not occur for Co^{2+} ion at modest concentrations.

Co-based films electrodeposit from unbuffered electrolyte (SO_4^{2-}, NO_3^-, ClO_4^-) solutions containing high concentrations of Co^{2+} ion (Co−X films).[10] A film forms on a nickel foil substrate[11] upon controlled current electrolysis ($i_a = 8$ mA/cm^2) of 500 mM $Co(SO_4)$ in reagent grade water in a three-electrode single-compartment cell.[12] Upon conclusion of electrolysis, the working electrode was placed in fresh electrolyte solution (0.1 M K_2SO_4, pH 7.0) containing no Co^{2+}. Electrolysis was initiated with stirring for 1 h at 1.3 V vs NHE using the standard two-compartment cell separated by a glass frit (as used for all previously described experiments). The current density traces obtained over this time are displayed in Figure 7. The current rapidly declines to 70 μA/cm^2 after 1 min and continues to diminish over the course of electrolysis to 36 μA/cm^2 after 1 h. For side-by-side comparison, a catalyst film was prepared on a nickel foil substrate by controlled potential electrolysis (1.40 V) of 0.5 mM Co^{2+} in Pi electrolyte solution. Upon conclusion of electrolysis, the electrode was placed in fresh Pi electrolyte solution containing no Co^{2+}. Electrolysis was initiated for 1 h at 1.3 V vs NHE and the same electrode geometry and stir rate was used as chosen for electrolysis in unbuffered solution. The current density trace is shown in Figure 7. Unlike Co−X systems, the current of the Co−Pi system remains stable at ∼1 mA/cm^2 over the entire course of the electrolysis.

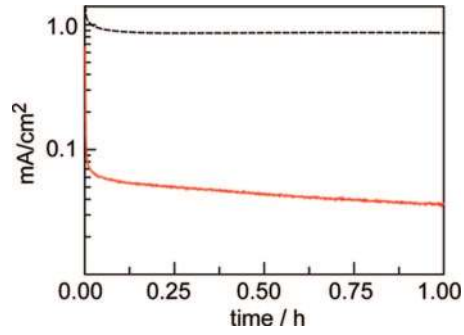

Figure 7. Controlled potential electrolysis at 1.3 V of a catalyst film operated in 0.1 M Pi electrolyte, pH 7.0 (- - -, black), and 0.1 M K_2SO_4, pH 7.0 (—, red). Catalysts deposited from Pi electrolyte and K_2SO_4 electrolyte respectively (see Supporting Information).

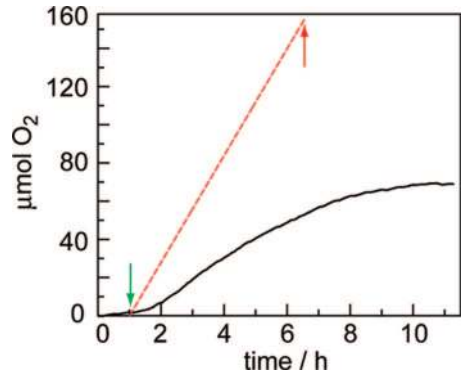

Figure 8. Faradaic efficiency of a single-compartment bulk electrolysis at 0.5 mA/cm^2 constant current. O_2 detected by fluorescence sensor (—, black) and theoretical O_2 trace assuming 100% Faradaic efficiency (- - -, red). Green and red arrows indicated start and end of electrolysis, respectively. Conditions: 0.1 M K_2SO_4 electrolyte, pH 7.0. Catalyst prepared from 0.1 M K_2SO_4 electrolyte, pH 7.0, 500 mM Co^{2+}.

Electrolytes possessing poor buffering capacity lead to diminished activity (vide supra) and to large pH gradients across a two-compartment cell. The pH drop may be circumvented by utilizing a single-compartment cell for water oxidation. To assess the Faradaic efficiency of a single-compartment setup, a Co−X film prepared from 500 mM $CoSO_4$ solutions as described above was electrolyzed using a three-electrode configuration in a single-compartment cell containing 0.1 M K_2SO_4 at pH 7.0. Evolved O_2 was detected by direct fluorescence-based sensing (Figure 8). Throughout the course of electrolysis, the amount of O_2 evolved is significantly attenuated relative to the amount of O_2 expected on the basis of 100% Faradaic efficiency.

Water Oxidation from Salt Water. Catalyst function does not require pure water. Controlled potential electrolysis of a Co−Pi film at 1.3 V in Pi electrolyte containing 0.5 M NaCl reveals sustained current densities greater than 0.9 mA/cm^2 (Figure S12). These current densities are comparable to those observed in the absence of NaCl, suggesting that chloride anions do not inhibit O_2 evolving catalysis (vide infra). EDX analysis of a film used for prolonged (16 h, 76.5 C passed) electrolysis in the presence of 0.5 M NaCl reveals that Co and P are retained in a ratio similar to that of the parent film.[6] In addition, EDX analysis also indicates significant incorporation of Na^+ ion, but only minimal incorporation of Cl^- (Na/Cl = ∼6:1), suggesting significant exchange of Na^+ ion for K^+ ion (Figure 9).

(10) Suzuki, O.; Takahashi, M.; Fukunaga, T.; Kuboyama, J. U.S. Patent 3,399,966, September 3, 1968.
(11) Nickel was chosen as the substrate because Co−X films exhibited more robust adhesion to the Ni foil substrate relative to ITO.
(12) Deposition from a standard two compartment cell using 500 mM Co^{2+} resulted in significant Co^{2+} precipitation in the auxiliary chamber as a result of pH increases associated with H_2 evolution at the cathode (see Figure S14).

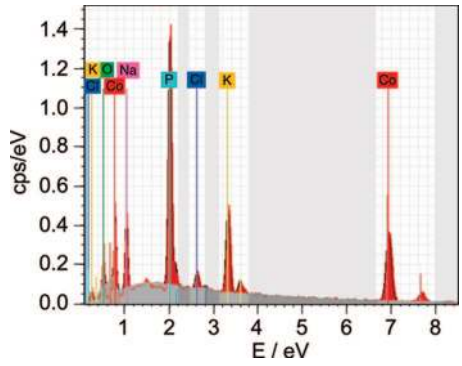

Figure 9. EDX histogram of a catalyst film after 16 h (76.5 C passed) of electrolysis in 0.5 M NaCl, 0.1 M KPi electrolyte, pH 7.0. $V_{appl} = 1.30$ V; cps = counts per second. Catalyst prepared from 0.1 M KPi electrolyte, pH 7.0, 0.5 mM Co^{2+}.

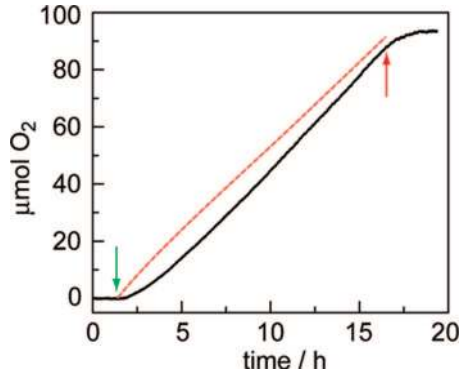

Figure 10. O_2 detected by fluorescence sensor (—, black) and theoretical O_2 trace assuming 100% Faradaic efficiency (- - -, red). Green and red arrows indicate start and end of electrolysis, respectively. Conditions: 0.1 M KPi electrolyte, pH 7.0, 0.5 M NaCl, $V_{appl} = 1.30$ V, no compensation for IR drop. Catalyst prepared from 0.1 M KPi electrolyte, pH 7.0, 0.5 mM Co^{2+}.

Noting the stability of the film in chloride-containing electrolyte, we quantified the Faradaic efficiency of water oxidation in this medium using fluorescence-based sensing of evolved O_2. Figure 10 shows the amount of oxygen produced at 1.30 V vs that expected for O_2 production with 100% Faradaic efficiency. The observed O_2 signal rises shortly after initiation of electrolysis as oxygen saturates the solution and fills the headspace, and hence the offset. The observed O_2 signal rises throughout the electrolysis (15 h) and plateaus upon termination of electrolysis at a value in accordance with the net current passed in the experiment (35.3 C, 91.4 μmol O_2). These results show that water oxidation to O_2 predominates (100% $\pm$ 5%) from salt solutions. This property of the system is further corroborated by direct quantification of oxidized chloride species (HOCl and OCl^-). A Co−Pi film was operated in the presence of 0.5 M NaCl for 16 h (76.5 C passed) at 1.30 V and then the solution was analyzed for hypochlorite using a standard *N*,*N*-diethyl-*p*-phenylenediamine titrimetric assay.[13] We observe 9.3 μmol of oxidized chloride species, which accounts for 1.80 C or 2.4% of the total current passed in the experiment. To exclude the possibility of Cl_2 production in this medium, the evolved gases were analyzed in real time by an in-line mass spectrometer. The only gas detected was O_2, and no isotopes of Cl_2 rose above the baseline level during the course of the experiment (6 h) (Figure S13).

Discussion

Electrolyte is a crucial determinant in the formation, activity and selectivity of self-assembled cobalt-based electrocatalysts for water oxidation. In the absence of suitable electrolytes, the generation of oxygen at appreciable activities from neutral water under ambient conditions cannot be achieved.

Large catalytic waves for water oxidation are observed from CVs of low concentrations of Co^{2+} (0.5 mM Co^{2+}) in solutions of Pi, MePi, or Bi electrolytes. Prior to the onset of catalytic current (Figure 1), an anodic wave is observed in the CV that is consistent with a $Co^{3+/2+}$ couple. The observed potential for this couple is well below that of $Co(OH_2)_6^{3+/2+}$ (1.86 V) but is similar to the 1.1 V potential estimated for the $Co(OH)_2^{+/0}$ couple.[14] As Figure 2 shows, the catalytic wave is preserved upon the placement of the once anodically scanned electrode in a fresh electrolyte solution containing no Co^{2+} cation. Polishing the electrode restores a clean background in the CV, indicating that a catalytically competent species electrodeposits immediately following oxidation of Co^{2+} to Co^{3+} at modest potentials. This behavior is in sharp contrast to CV traces obtained from Co^{2+} in electrolytes of poor proton-accepting abilities. In electrolytes such as SO_4^{2-} and ClO_4^- (Figures 6 and S11), no electrochemical features of significance are observed above background for solutions containing 0.5 mM Co^{2+}. Only when the Co^{2+} ion concentration is increased by 2 orders of magnitude is a slight enhancement in current observed near the solvent window at 1.56 V. This current enhancement is anodically shifted >150 mV relative to the corresponding wave in Pi at drastically lower Co^{2+} concentration. Electrolyte promotes catalyst formation; in the absence of an effective proton acceptor at a given pH, the formation of a catalyst film is significantly inhibited.

Whereas an active catalyst can be generated on an anodic single scan, films of desired thickness may be prepared on conducting electrodes (metal or semiconductor) by controlled potential electrolysis of 0.5 mM Co^{2+} solutions of Pi, MePi, and Bi. The bulk composition of the films, as determined by elemental analysis and corroborated by EDX, reveals a higher Co/P ratio for Co−MePi (~5:1) relative to the Co/P ratio of ~2:1 observed for Co−Pi. An even lower anion content is observed for Co−Bi which exhibits a Co/B ratio of 10:1. We note that the anion composition is balanced by a monovalent cation in all cases, regardless of the Co-to-anion ratio. The disparate anion incorporation into the bulk material is not reflected in altered activity, suggesting that a common Co−oxide unit effects catalysis in all films. The active unit is <5 nm in dimension, as evidenced by the absence of crystalline features in the power X-ray diffraction pattern (Figure S4) and diffraction patterns in the TEM (Figure S5). This is in contrast to the structural properties of Co−X materials, which are asserted[10] to exhibit long-range ordering corresponding to CoO_x crystallites.

An electrolyte environment that has good proton-accepting properties is required for sustained catalyst activity at appreciable current density. The Pi electrolyte is an efficient proton carrier, and it preserves a stable local pH environment required for high catalytic activity. In addition, it functions as an acceptor of the

(13) Eaton, A. D.; Clesceri, L. S.; Rice, W. E.; Greenberg, A. E. *Standard Methods for the Examination of Water and Wastewater*, 21st ed.; American Public Health Association, American Water Works Association, Water Pollution Control Federation: Washington, DC, 2005; Chapter 4.

(14) Brunschwig, B. S.; Chou, M. H.; Creutz, C.; Ghosh, P.; Sutin, N. *J. Am. Chem. Soc.* **1983**, *105*, 4832.

protons furnished from water oxidation and participates in the PCET activation of oxygen.[15] Alternative electrolytes are able to support catalysis as long they have sufficient proton-accepting capacity in the pH regime of interest and are stable under the conditions of catalysis. MePi and Bi electrolytes meet these criteria at pH 8.0 and 9.2, respectively. Co−MePi and Co−Bi films support catalytic activity comparable to that observed for Co−Pi, as demonstrated by their associated Tafel behaviors (Figure 5). We envision other oxidation resistant buffers would also function in a similar capacity enabling robust water oxidation catalysis over a large pH range. MePi offers an advantage in being able to sustain higher concentrations of Co^{2+} relative to either Pi or Bi. Despite the low concentration of PO_4^{3-} expected in Pi electrolytes at pH 7.0, the low solubility of $Co_3(PO_4)_2$ ($K_{sp} = 2.05 \times 10^{-35}$) elicits the slow precipitation of Co^{2+} from solution.[16] Precipitation is instead averted in MePi electrolyte, where Co^{2+} is indefinitely soluble at 2 mM.

In the absence of efficient proton-accepting electrolytes (e.g., SO_4^{2-}, NO_3^-, ClO_4^-), proton buildup results in dramatically reduced current densities that decay over time. In solutions of these counteranions, the Co−oxide catalyst is the best base and consequently the catalyst is subject to corrosion induced by the protons produced from water splitting. In addition, catalyst activity is inhibited by changes in local and bulk pH. Bulk pH can reach a steady-state value in a single-compartment cell. However, as expected and verified by the data in Figure 8, significant short circuit current from redox cycling between the anode and cathode stifles oxygen production. For these reasons, a sustainable water-splitting reaction cannot be achieved by Co-based catalysts in the absence of proton-accepting electrolytes.

The ability of the electrolyte to maintain the pH during water oxidation is manifested in a robust and functional catalyst in the presence of 0.5 M NaCl. Direct measurement of Faradaic efficiency and titrimetry of chloride oxidation products establishes that Co−Pi is able to produce oxygen from salt water at current efficiencies commensurate with those observed for pure water. At pH 7.0, the $HOCl/Cl^-$ redox process has a thermodynamic potential of 1.28 V, 0.46 V beyond the thermodynamic potential for water oxidation to O_2. With decreasing pH, the oxidation of Cl^- becomes more thermodynamically competitive with water oxidation. Therefore, in the absence of proton-accepting electrolytes (such as Co−X), chloride oxidation will interfere with water oxidation. The ability of the Pi electrolyte to preserve the pH of the solution allows O_2 production to outcompete Cl^- oxidation.

Conclusion

The observations reported herein highlight several attractive properties of the new oxygen-evolving cobalt catalyst for water oxidation under benign conditions. High activities for water oxidation demand the involvement of a proton-accepting electrolyte. The electrolyte facilitates catalyst formation, allows for high activity for water oxidation, and preserves the catalyst during turnover. By maintaining pH with the electrolyte, the catalyst is able to produce oxygen from high concentrations of salt water at current efficiencies commensurate with those observed for pure water.

Water splitting is a solar energy storage mechanism of sufficient scale to address future global energy needs.[17] As we have emphasized, the conditions under which water splitting is performed will determine how solar energy is deployed.[6] Commercial electrolyzers are extremely efficient and operate at current densities as high as 1 A/cm^2. However, commercial electrolyzers operate under harsh conditions and accordingly they are difficult to maintain and costly to engineer. Moreover, the current density of commercial electrolyzers is at variance with many applications of nonconcentrated solar energy. The cobalt catalyst described herein is better matched to the 10−20 mA/cm^2 output of a conventional photovoltaic device that provides the required voltage for water-splitting.[18] With an improved cell design, these current densities will be achieved with the cobalt catalyst. Therefore, the Co−Pi catalyst is well adapted for the design of inexpensive and highly manufacturable water-splitting systems. These systems extend beyond an electrolyzer. We demonstrate here that an active catalyst forms immediately following oxidation of Co^{2+} in solution suggesting that the cobalt catalysts are amenable to rapid, ultrathin film electrodeposition on a wide array of substrates with complicated geometries and large surface areas, such as those involving nanostructured semiconducting materials.[19−21] Of added potential, since water splitting is not performed in highly acidic or basic conditions, the catalyst is amenable to integration with charge-separating networks comprising protein,[22,23] organic, and inorganic[24−26] constituents. In these systems, the one-photon, one-electron charge separation can be accumulated by the catalyst to attain the 4 redox equivalents needed for water splitting. The ease of implementation of the catalyst with a diverse array of substrates suggests that the catalyst will be of interest to many in their endeavors to store solar energy by water splitting.

Acknowledgment. We thank Drs. Bruce Brunschwig, Harry Gray, Nathan Lewis, and Bruce Parkinson for their thoughtful comments. This research was supported by a Center for Chemical Innovation of the National Science Foundation (Grant No. CHE-0533150) and a grant from the Chesonis Family Foundation. Grants from the NSF also provided instrument support to the DCIF at MIT (CHE-9808061, DBI-9729592). Y.S. gratefully acknowledges the Department of Defense for a (NDSEG) predoctoral fellowship. We thank M. W. Kanan for collecting powder X-ray diffraction spectra and for many productive discussions.

Supporting Information Available: Full experimental details, additional SEM and TEM images, EDX and ^{31}P spectra, and MS traces. This material is available free of charge via the Internet at http://pubs.acs.org.

JA807769R

(15) Irebo, T.; Reece, S. Y.; Sjödin, M.; Nocera, D. G.; Hammarström, L. *J. Am. Chem. Soc.* **2007**, *129*, 154622.
(16) Lide, D. R. *CRC Handbook of Chemistry and Physics*, 77th ed.; CRC Press: Boca Raton, FL, 1996; pp 8−91.
(17) Nocera, D. G *ChemSusChem* **2009**, in press.
(18) Green, M. A.; Emery, K.; Hishikawa, Y.; Warta, W. *Prog. Photovolt. Res. Appl.* **2009**, *17*, 85.
(19) Kay, A.; Cesar, I.; Grätzel, M. *J. Am. Chem. Soc.* **2006**, *128*, 15714.
(20) Maiolo, J. R.; Kayes, B. M.; Filler, M. A.; Putnam, M. C.; Kelzenberg, M. D.; Atwater, H. A.; Lewis, N. S. *J. Am. Chem. Soc.* **2007**, *129*, 12346.
(21) Yang, F.; Forrest, S. R. *ACS Nano* **2008**, *2*, 1022.
(22) Shih, C.; Museth, A. K.; Abrahamsson, M.; Blanco-Rodriguez, A. M.; Di Bilio, A. J.; Sudhamsu, J.; Crane, B. R.; Ronayne, K. L.; Towrie, M.; Vlcek, A., Jr.; Richards, J. H.; Winkler, J. R.; Gray, H. B. *Science* **2008**, *320*, 1760.
(23) Stubbe, J.; Nocera, D. G.; Yee, C. S.; Chang, M. C. Y. *Chem. Rev.* **2003**, *103*, 2167.
(24) Fukuzumi, S. *Phys. Chem. Chem. Phys.* **2008**, *10*, 2283.
(25) Hambourger, M.; Moore, G. F.; Kramer, D. M.; Gust, D.; Moore, A. L.; Moore, T. A. *Chem. Soc. Rev.* **2009**, *38*, 25.
(26) Flamigni, L.; Collin, J.-P.; Sauvage, J.-P. *Acc. Chem. Res.* **2008**, *41*, 857.